Acta Chemica Scandinavica, 1998: 52: 1359–1372
Printed in UK – all rights reserved

ACTA
CHEMICA SCANDINAVICA
ISSN 0904-213X

The Conformers of Bromomethyl Dimethyl Fluorosilane Studied by Vibrational Spectroscopy and *ab Initio* Methods

Heidi M. Jensen,[a] Gamil A. Guirgis,[b] Peter Klaeboe,*,[a] Claus J. Nielsen[a] and Valdemaras Aleksat

[a]Department of Chemistry, University of Oslo, PO Box 1033, 0315 Oslo, Norway and [b]Bayer Corporation, Bushy Park Plant, Research and Development Department, Charleston, SC 29208, USA

Jensen, H. M., Guirgis, G. A., Klaeboe, P., Nielsen, C. J. and Aleksa, V. The Conformers of Bromomethyl Dimethyl Fluorosilane Studied by Vibrational Spectroscopy and *ab Initio* Methods. – Acta Chem. Scand. 52: 1359–1372. © Acta Chemica Scandinavica 1998.

Bromomethyl dimethyl fluorosilane ($CH_2Br(CH_3)_2SiF$) has been synthesized for the first time. Raman spectra of the liquid were obtained at various temperatures between 295 and 163 K, and spectra of the amorphous and crystalline solids were recorded. The infrared spectra of the vapor and of the amorphous and crystalline states at liquid nitrogen temperature were obtained. IR spectra of the compound, isolated in argon and nitrogen matrices, were recorded at 5 and 15 K.

The compound is present as *anti* and *gauche* conformers in the vapor and in the liquid states. Five infrared and eight Raman bands present in these phases vanished upon crystallization. Raman temperature studies in the liquid gave a $\Delta_{conf}H(anti-gauche)$ value of 0.4 ± 0.3 kJ mol^{-1}; *gauche* was the low-energy conformer and was also present in the crystal. The infrared bands vanishing in the argon and nitrogen matrix spectra after annealing to ca. 25–28 K suggested that the *anti* conformer had a lower energy than *gauche* in both matrices. The conformational barrier was estimated to be 6–7 kJ mol^{-1}.

Ab initio calculations on different levels of approximation gave optimized geometries, infrared and Raman intensities and vibrational frequencies for the *anti* and *gauche* conformers. All calculations predicted the *anti* as the low-energy conformer. After scaling, a reasonably good agreement between the experimental and calculated wavenumbers for the two rotamers was obtained.

Bromomethyl dimethyl fluorosilane, $CH_2Br(CH_3)_2SiF$, abbreviated as BDFS, has been synthesized for the first time. The molecule can exist in two conformations, *anti* and *gauche*, as shown in Fig. 1. The infrared and Raman spectra of BDFS were investigated among a series of six halomethyl dimethyl halosilanes, $CH_2X(CH_3)_2SiY$ (X = Cl, Br; Y = H, F, Cl). Various saturated[1–3] and unsaturated[4–6] compounds with conformational equilibria containing one silicon atom have been studied, and the vibrational spectra of molecules with two[7–9] and three[10] silicon atoms have very recently been reported.

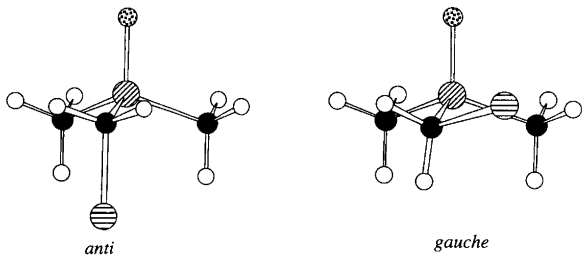

Fig. 1. The *anti* and *gauche* conformers of bromomethyl dimethyl fluorosilane (BDFS).

The vapor, amorphous and crystalline samples of BDFS were recorded in the middle (MIR) and far-infrared (FIR) regions. The infrared matrix isolation technique was employed to obtain spectra of the compound trapped in argon and nitrogen matrices. The narrow bandwidths observed in the matrix spectra are an advantage for interpreting conformational equilibria. They often make it possible to distinguish neighboring bands of different conformers which overlap in spectra of the vapor and liquid. Moreover, by appropriate annealing the conformational barriers can frequently be estimated from the matrix spectra.

Raman spectra of the liquid, including polarization measurements, were obtained. Spectra of the liquid were recorded at different temperatures, some of them far below the melting point made possible by the large

* To whom correspondence should be addressed.
† Permanent address: Department of General Physics and Spectroscopy, Vilnius University, Vilnius 2734, Lithuania.

supercooling. Raman spectra of BDFS as a crystal were observed using different cooling techniques. Moreover, the conformational energies, the structure, the force constants and the infrared and Raman intensities were calculated by *ab initio* methods. Our complete results for BDFS are given in the present article, while in a preliminary communication certain spectroscopic features and results from quantum chemistry have already been reported.[11]

Experimental

Sample preparation. The sample of BDFS was prepared for the first time by reaction of bromomethyl dimethyl chlorosilane[12] with freshly sublimed antimony trifluoride at room temperature for 1 h. The compound was distilled in a low-temperature, low-pressure fractionation column and the purity was checked by mass spectrometry (m.p. 208 K). No apparent impurities were observed in the vibrational spectra.

Raman spectral measurements. The Raman spectra were obtained using a Dilor RTI-30 spectrometer (triple monochromator) and recorded digitally. An argon ion laser from Spectra Physics (model 2000) was employed using the 514.5 nm line for excitation. Spectra of the liquid were obtained at room temperature and at 12 temperatures between 293 and 163 K in a capillary tube of 2 mm inner diameter surrounded by a Dewar, cooled by gaseous nitrogen evaporated from a reservoir.[13] These spectra were employed for calculating the enthalpy difference $\Delta_{conf}H$ between the conformers in the liquid. BDFS and the related halomethyl dimethyl halosilanes all had unusually large hysteresis (undercooling) and it was sometimes possible to study the liquid 50–60 K below the freezing point (ca. 208 K). The crystallization occurred spontaneously around 140 K, and an anisotropic crystal containing only one conformer was obtained. In other experiments the vapor of BDFS was condensed on a copper finger at 80 K. An amorphous phase was first formed and the spectrum recorded was quite similar to that of the liquid. After annealing to ca. 140–160 K a crystalline phase was obtained giving the same spectrum as the crystal formed from the liquid at 140 K. When recooled to 80 K much sharper Raman bands were observed than in the spectra of the amorphous solid.

Infrared spectral measurements. The infrared spectra were recorded on a variety of Fourier transform spectrometers: a Bruker model IFS-88 (4000–450 cm^{-1}), a Nicolet model 800 (4000–450 cm^{-1}) and a Perkin-Elmer model 2000 (4000–450 cm^{-1}) in MIR and on a Bruker IFS-113v vacuum spectrometer in FIR (600–50 cm^{-1}). Beamsplitters of Ge substrate on KBr were employed in MIR, 3.5 and 12 μm Mylar in addition to a metal mesh beamsplitters were used in FIR. The vapor was investigated in cells with KBr (10 cm) and polyethylene windows (20 cm). The amorphous and crystalline solids were studied on a CsI window and on a wedge-shaped window of silicon, cooled with liquid nitrogen, for the MIR and FIR, respectively.

The sample was diluted with argon or nitrogen (1 : 500 and 1 : 1000) and deposited on a CsI window at either 5 or 15 K on a Displex cryostat from APD (model HS-4) with a three-stage cooling system. The samples were first heated to various temperatures below 20 K in order to remove site effects in the matrices. Subsequently they were annealed in steps of 3–5 K to a maximum of 36 K in argon and 33 K in nitrogen in periods from 10 min to 1 h. At still higher temperatures the inert gases have a pressure higher than 10^{-3} Torr, which is not feasible in the cryostat. Temperatures at which the matrices turn 'soft' and diffusion starts are estimated to be ca. 35 and 31 K for argon and nitrogen, respectively. After each annealing the window was recooled to 5 K and the spectra were recorded.

Results

Raman spectral results. Raman spectra below 1500 cm^{-1} of the liquid at ambient temperature in two polarization directions are presented in Fig. 2; spectra of the liquid and of an annealed crystalline solid are compared in Fig. 3. As is apparent, some of the bands present in the Raman spectrum of the liquid disappear in the spectrum of the crystal. Generally, the same bands are also absent in the corresponding infrared spectrum of a crystalline solid (see below). These vanishing bands are assigned to the second conformer which is absent in the crystal. To be discussed below, it is assumed that the conformer present in the crystal is *gauche*. The number of vanishing bands (7 or 8) is small, and lower than those generally found in the corresponding ethanes. Thus, most of the fundamentals of one conformer overlap those of the other. This conclusion agrees with the earlier results obtained for silanes with conformational equilibria,[1–3] and is probably due to the relatively weak interaction between the substituents and the long Si–C distance in these molecules compared to the C–C distance in ethanes.

Raman spectra of the liquid were recorded at 12 temperatures between 295 and 163 K. Small intensity variations with temperature of certain bands relative to neighboring bands were observed and interpreted as a displacement of the conformational equilibrium. The Raman bands which vanished upon crystallization belong to one conformer, and they were paired with other bands (often neighbors) which remained in the crystal. However, it is *a priori* quite uncertain if the corresponding liquid bands are characteristic of only one conformer or if they belong to overlapping bands of both conformers. In some cases the results of the force constant calculations strongly suggest that they may originate from one conformer only.

In order to determine the enthalpy difference from the variable temperature spectra the bands of the different

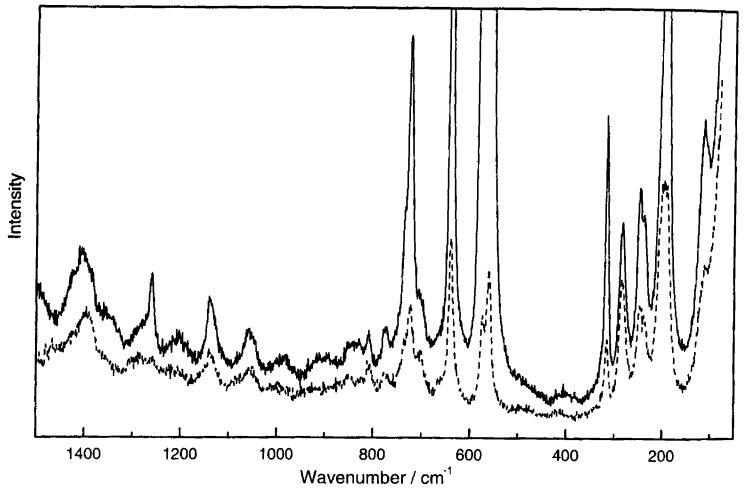

Fig. 2. Raman spectra (1500–100 cm^{-1}) of BDFS as a liquid in two polarization directions at ambient temperature. Solid line, parallel component; dashed line, perpendicular component.

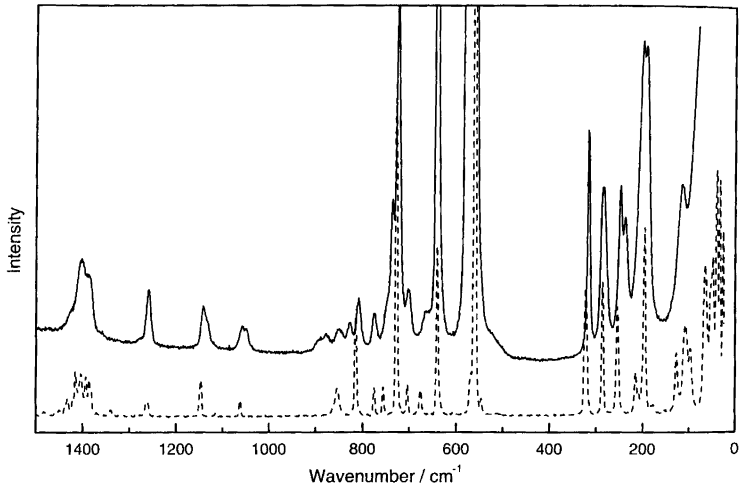

Fig. 3. Raman spectra (1500–40 cm^{-1}) of BDFS as a liquid at 298 K (solid line) and as crystalline solid at 80 K (dashed line).

conformers should both have reasonably high intensities, they should be situated on a flat background and not overlap other bands in the spectra. Moreover, they must be 'pure', meaning that their intensities should be due to one conformer only, with no contribution, either from fundamentals or from combination bands, of the other conformer. For this reason, we decided to carry out independent calculations of $\Delta_{conf}H$ from each pair. Considerable discrepancies might occur between the $\Delta_{conf}H$ values obtained from different band pairs, indicating either a poor signal-to-noise ratio, overlapping bands or an ill-defined background. Eventually, one or both bands of the pair may be contaminated with the other conformer, meaning a superposition between a fundamental of one conformer and a fundamental, combination band or overtone belonging to the other conformer.

The intensities of each band pair were fitted to the van't Hoff equation: $\ln\{I_{anti}(T)/I_{gauche}(T)\} = -\Delta_{conf}H/RT + \text{constant}$; where I_{anti}/I_{gauche} is the ratio in peak heights or integrated areas and it is assumed that $\Delta_{conf}H$ is constant with temperature. Both peak heights and integrated band areas were attempted for determining band intensities. However, in spite of careful curve resolution and determination of band areas with advanced computer programs, the calculations based upon band areas invariably showed a large scatter. Table 2 summarizes the results of the van't Hoff plots based upon peak height measurements; the average value $\Delta_{conf}H = 0.4 \pm 0.3$ kJ mol^{-1} was derived from these data.

All together six pairs of bands were treated in the van't Hoff plots: 198*/237, 576*/561, 736*/723, 828*/810 and 1132*/1142 cm^{-1} (values for the liquid), in which the band fitted with asterisk vanished in the crystal. The pair 198*/191 cm^{-1} behaved significantly differently from the other band pairs, and was for this reason not employed in the calculations. The bands at 576*/561 cm^{-1} were both very intense in the Raman region and seemed well suited for quantitative calculations. However, this pair gave a somewhat lower value ($\Delta_{conf}H = 0.13$ kJ mol^{-1}) than the average. The mean

Table 1. Infrared and Raman spectral data[a] for bromomethyl dimethyl fluorosilane (BDFS).

IR					Raman				
	Matrix		Solid			Solid		Interpretation	
Vapor	Argon (5 K)	Nitrogen (5 K)	Amorphous (80 K)	Crystal (80 K)	Liquid	Amorphous (80 K)	Crystal (80 K)	*gauche*	*anti*
3008 vw			3002 vw	3002 m	3004 m	3004 vw	3004 m	ν_1	ν_1
		2991 m			2995 m,D				
2976 m	2985 m 2981 m	2986 s		2977 w	2971 w	2976 w	2977 w	ν_2	ν_2
		2976 s	2973 m			2974 m			
		2966 w	2967 m,br	2965 w	2965 m,P	2967 m	2968 m	ν_3	ν_3
	2963 w	2963 m							
	2959 m	2962 m		2961 m			2961 s		
	2957 w	2959 m							
	2954 w								
2960 m 2955 m 2951 m	2951 m	2957 m↓	2944 w	2948 w	2943 m,P	2942 m	2946 vs	$\nu_4\nu_5$	$\nu_4\nu_5$
2946 w	2943 m								
2943 w	2938 w				2920 m,P				
2915 w	2920 w	2917 w	2905 w	2905 w	2910 s,P	2910 m	2910 m	$\nu_6\nu_7\nu_8$	$\nu_6\nu_7\nu_8$
2862 w	2888 w						2864 w		
2853 w		2854 w	2853 vw	2853 vw			2850 vw		
2800 vw		2789 w	2785 vw	2785 vw	2791 vw		2780 vw		
				1479 w	1480 w		1478 w		
				1474 w	1477 w	1476 vw	1477 vw		
1469 w	1456 m 1455 m		1457 m	1462 m	1465 w,D			ν_9	ν_9
				1446 m			1445 w		
	1437 m		1432 m	1434 m			1432 w		
1424 w	1428 m		1419 w		1425 w	1425 w	1427 w	ν_{10}	ν_{10}
						1418 vw	1417 w		
	1413 m		1412 w,br	1409 m 1407 m	1405 s,P	1407 m	1412 w	$\nu_{11}\nu_{12}$	$\nu_{11}\nu_{12}$
	1405 w		1404 w	1401 w		1399 vw			
1397 m	1400 m		1394 w		1390 m		1402 w 1398 m	ν_{13}	ν_{13}
	1383 m	1381 m	1381 m,br	1382 w 1381 m			1381 w 1377 w	comb.	
	1379 m								
	1352 w	1363 w	1365 w	1366 vw	1360 vw,P	1358 vw		comb.	
				1337 vw			1335 vw		
		1314 w	1308 w						
	1287 w	1285 w			1289 vw				
		1281 m			1285 vw				
	1276 m↑	1274 m	1276 m	1279 m	1277 vw		1277 vw	ν_{14}	ν_{14}
	1270 m↓	1270 m							
	1269 m								
	1262 vs								
1267 m	1259 vs	1260 s	1257 vs	1259 vs	1260 m,P	1260 w	1260 m 1258 m	ν_{15}	ν_{15}
	1251 m	1251 m		1252 vs					
		1250 m							
	1140 m↓	1142 m	1142 m	1146 m 1143 s	1141 w,P	1140 m	1142 w	ν_{16}	
		1141 m							
		1139 m							
	1137 m↑	1137 s							
	1136 m								
1139 m 1135 m 1131 m	1134 m	1134 s	1134 m	*	1132 m	1130 w	*		ν_{16}
1127 m	1131 s	1132 s							
	1129 m↓								
	1123 w								

Table 1. (Continued.)

IR					Raman				
	Matrix		Solid			Solid		Interpretation	
Vapor	Argon (5 K)	Nitrogen (5 K)	Amorphous (80 K)	Crystal (80 K)	Liquid	Amorphous (80 K)	Crystal (80 K)	*gauche*	*anti*
				1112 w			1111 vw		
1098 w		1100 w	1093 w	1093 w					
1089 vw				1084 vw	1086 vw				
	1061 w	1079 m		1077 vw					
	1057 w	1054 m							
	1053 w								
1047 m	1048 m	1049 s, 1048 s		1058 s, 1057 s	1057 m,P	1059 m	1059 m	ν_{17}	
	1046 m								
	1044 s		1055 m,br	*	1049 m		*		ν_{17}
	1042 m								
	1038 m								
	1036 m								
986 vw				985 w	989 vw,D				
960 vw				966 w	960 w,D			comb.	
950 w				946 w					
912 m				923 vw					
901 m	903 s↑								
	900 s↑	900 s↓		*	895 vw		*		comb.
	889 vs	887 m	888 m	*	889 vw		*		comb.
	885 s								
895 vs	882 m	879 s	872 s	*	877 w	878 w	*		ν_{18}
	858 m								
	856 vs	854 s		854 vs	853 w,P	849 vw	852 w	ν_{18}	
	849 vs	849 s							
852 s	842 m, 838 m	840 m, 835 m	849 s	844 vs				ν_{19}	ν_{19}
832 m	830 s, 827 vs	830 s↑, 827 s↑	827 s	826 s	828 w	828 w	*		ν_{20}
	822 m	822 m							
	817 m	818 m							
810 m	809 vs	809 s↓	809 s	812 s	810 w,P	810 w	810 w	ν_{20}	
	807 s								
	805 s			805 m					
	802 s	800 m,mt		800 m					
779 w	783 w, 775 s, 773 m, 772 m↓	779 s, 776 m, 773 s↑	775 s	775 s	775 w,P	772 w	771 w	ν_{21}	ν_{21}
	754 m	754 m							
	750 s	752 s							
750 w	746 m	749 s	750 m	752 m	753 vw	751 w	752 vw	ν_{22}	ν_{22}
	741 m	743 m							
	739 w	738 s							
740 w, 736 w	737 w	737 s↑	735 m	*	736 w	736 m	*		ν_{23}
731 w	734 m↓	734 m↓	723 m	723 m	723 m,P	724 s	724 m	ν_{23}	
700 w,br	719 w	696 w,br	698 m	698 m	700 m	700 m	700 w	ν_{24}	ν_{24}
665 vw	670 m		664 vw	671 w	665 w,sh		672 w	ν_{25}	ν_{25}
	646 w								
646 w, 642 w, 637 w A	643 s, 642 m, 640 m, 637 s	641 s	637 m	637 m	641 s,P	643 m	637 s	ν_{26}	ν_{26}
	580 s↑	580 s↑							
577 m,A	578 s↑	577 s↑	574 m	*	576 s,P	575 s	*		ν_{27}
	573 m	572 m							
560 m	563 w	563 w↓	559 m	559 m	561 vs,P	560 vs	565 w, 557 vs, 536 w	ν_{27}	

Table 1. (Continued.)

IR					Raman				
	Matrix		Solid			Solid		Interpretation	
Vapor	Argon (5 K)	Nitrogen (5 K)	Amorphous (80 K)	Crystal (80 K)	Liquid	Amorphous (80 K)	Crystal (80 K)	*gauche*	*anti*
	419 m,br	423 w 420 m 419 m		419 vw					
317 s			314 s	314 s	315 m,P	313 m	318 m 316 vw	ν_{28}	
			284 s	*	284 m,D	281 m	*		ν_{28}
281 s			274 s	278 s			276 m	ν_{29}	ν_{29}
			252 m	251 w,br	248 m,P	246 m	249 m	ν_{30}	
					237 m,P	235 m	*		ν_{30}
200 vw			209 w 203 w	213 w 206 w	210 w,sh	207 w	210 w 205 vw	ν_{31}	ν_{31}
					198 m,P	197 m,br	*		ν_{32}
					191 m,P		191 m	ν_{32}	
				176 vw			173 vw	ν_{33}	ν_{33}
							148 vw	ν_{34}	ν_{34}
			122 m	120 vw	115 m,P	115 w	123 w	ν_{35}	ν_{35}
101 m			100 w	109 m 101 m 92 m	85 m		92 w	ν_{36}	
							60 m	crystal	
66 w					53 m				ν_{36}
							35 m	crystal	
							21 m	crystal	

[a]Abbreviations: s, strong; m, medium; w, weak; v, very; sh, shoulder; br, broad; P, polarized; D, depolarized; A, B and C, infrared vapor contours; arrows pointing upwards or downwards denote bands which increase or decrease after annealing, respectively; asterisks signify bands which disappear on crystallization.

Table 2. Derived $\Delta_{conf}H$ from van't Hoff plots employing peak heights as intensity measures.

Band pair[a]	$\Delta_{conf}H$/kJ mol^{-1}	σ^b/kJ mol^{-1}
1132*/1142	0.27	0.08
828*/810	0.63	0.16
736*/724	0.90	0.11
576*/561	0.13	0.05
235*/249	0.27	0.10
Average	0.44	0.32

[a]Bands equipped with asterisk correspond to the high energy conformer in the liquid. [b]σ represents 1 standard deviation in the derived $\Delta_{conf}H$.

value of $\Delta_{conf}H$ (*anti*−*gauche*) was 0.4 ± 0.3 kJ mol^{-1} with *gauche* apparently being the low-energy conformer in the liquid (see below).

Infrared spectral results. An infrared survey spectrum of BDFS as a vapor in the 4000–400 cm^{-1} range at 7 Torr pressure is presented in Fig. 4. A vapor spectrum in FIR (600–50 cm^{-1}) at a pressure of 33 Torr is given in Fig. 5. The infrared spectra of the amorphous and crystalline solids at 80 K are found in Fig. 6 (1600–400 cm^{-1}) and in Fig. 7 (700–50 cm^{-1}). The infrared bands present in the amorphous solid, but vanishing in the crystal spectra after annealing, are the same as those disappearing in the crystal phases in the Raman spectra (see above). These bands also diminish in intensity at lower temperatures and therefore belong to the high-energy conformer in the liquid.

Additional infrared spectra of BDFS were recorded in argon and in nitrogen matrices (mixing ratios 1:500 and 1:1000) deposited both at 5 and 15 K. The quality of the infrared matrix spectra are often better when deposited at 15 K. However, in the case of very low conformational barriers the 5 K deposition temperature is advantageous to prevent instantaneous conformational conversion.

Survey infrared spectra (1500–400 cm^{-1}) of unannealed BDFS in an argon matrix, deposited at 5 K of the unannealed and annealed sample are shown in Fig 8. Supposedly, the conformational equilibrium of the vapor phase is maintained when the gas mixture is quickly frozen on the CsI window at 5 or 15 K, provided that the barrier to conformational equilibrium is above 3 and 5 kJ mol^{-1}, respectively.[14] Various spectral changes occur after annealing around 20 K. They are often different in argon and nitrogen matrices and interpreted as site effects due to relaxation of BDFS in the matrix cages. As expected, the changes are more prominent when depositions are carried out at 5 K than at 15 K. At higher annealing temperatures (20–37 K) changes were observed both in the argon and nitrogen matrix spectra

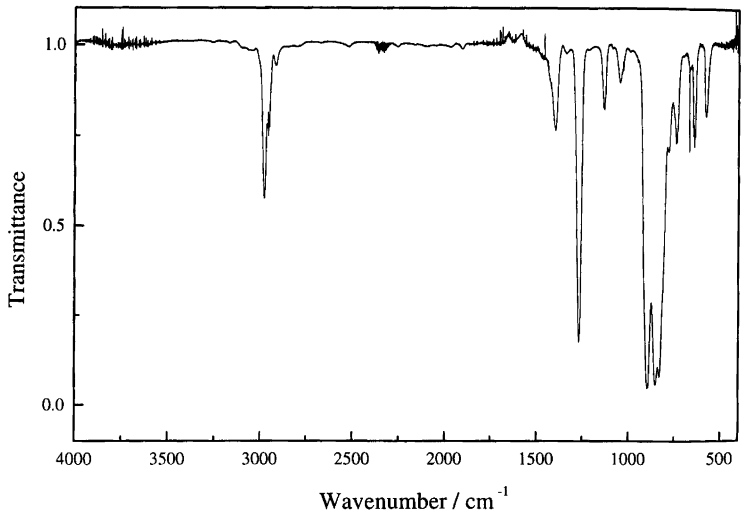

Fig. 4. Infrared spectrum (4000–400 cm^{-1}) of BDFS as a vapor, path length 10 cm at 7 Torr pressure.

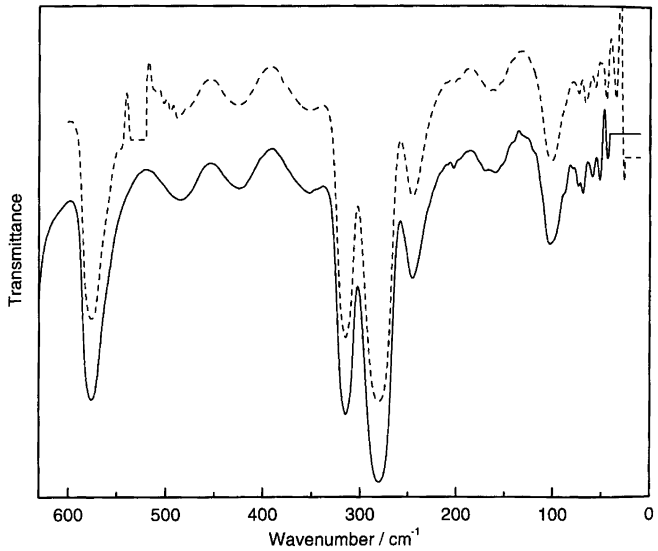

Fig. 5. Infrared spectrum (630–50 cm^{-1}) of BDFS as a vapor, path length 20 cm at 33 Torr pressure. Solid curve, spectrum obtained using a 3.5-μm mylar beamsplitter; dashed curve, spectrum obtained using a metal mesh beamsplitter.

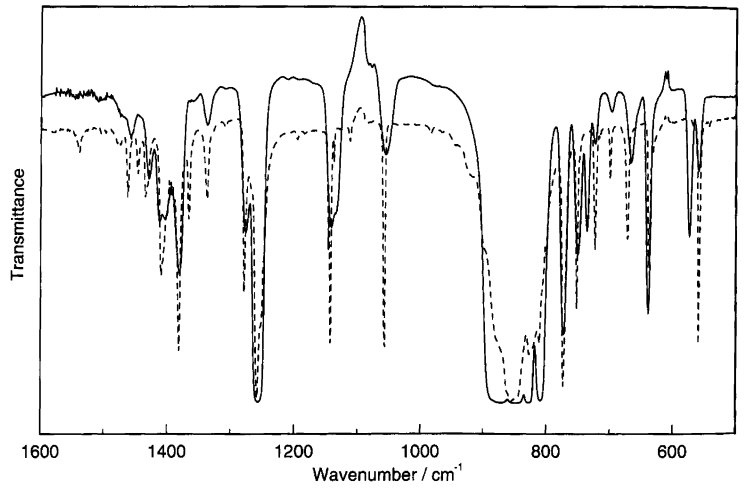

Fig. 6. Infrared spectra (1600–400 cm^{-1}) amorphous (solid line) and crystalline (dashed) solids of BDFS at 80 K.

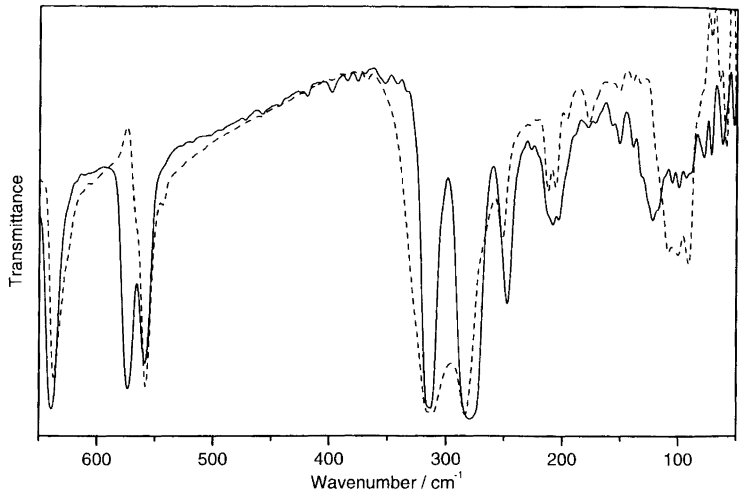

Fig. 7. Infrared spectra (650–50 cm^{-1}) of amorphous (solid line) and crystalline (dashed line) solids of BDFS at 80 K.

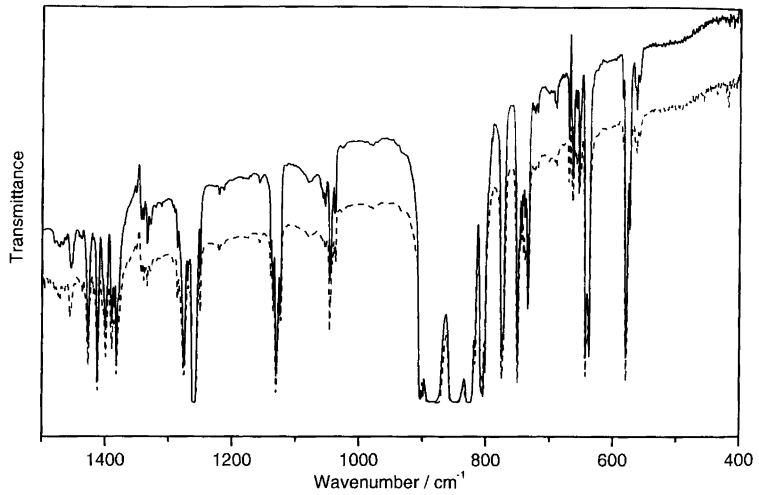

Fig. 8. Infrared spectra (1500–400 cm^{-1}) of BDFS in an argon matrix deposited at 5 K, unannealed sample, solid line; annealed to 34 K, dashed line.

which were correlated with conformational changes in BDFS. As an archetype, the bands at 830 and 827 cm^{-1} were enhanced compared to that at 809 cm^{-1} in nitrogen matrices after annealing to 32 K, as is apparent from Fig. 9. Another example is the doublet at 577 and 580 cm^{-1}, increasing in intensity compared to the band at 572 cm^{-1} after annealing. The same bands also changed intensities in argon matrices, as can be seen from Fig. 10. Other examples are the bands at 734 cm^{-1} diminishing in intensity compared to that at 773 cm^{-1} (nitrogen), and a band at 1140 cm^{-1} diminishing compared to that at 1137 cm^{-1} (argon).

It should be emphasized that the bands vanishing in the matrix spectra after annealing are not those that disappear on crystallization. On the contrary, they are present in both the infrared and Raman spectra of the crystals. Consequently, both the argon and nitrogen matrices stabilize a conformer which disappears in the crystal and which is also the high-energy conformer in the liquid. Hence, the high-energy conformer in the liquid is the low-energy conformer in both the argon and nitrogen matrices: the conformational stabilities in the liquid state and in the argon and nitrogen matrices are opposite. Quite similar observations were made for the related molecule chloromethyl dimethyl fluorosilane.[15] As discussed below, the conformer present in the crystal, which is also the low-energy conformer in the liquid and in the amorphous solid, is believed to be *gauche*.

The lowest annealing temperature at which the equilibrium of the solute molecule is displaced from the high- to the low-energy conformation was used for estimating the conformational barrier. For both matrices this temperature was ca. 32 K. From the curves correlating annealing temperature and activation energy/barrier height given by Barnes[14] the conformational barrier was estimated to be 6–7 kJ mol^{-1}. If secondary effects due to matrix viscosity or matrix–solute interactions are neglected, this barrier height may also be valid for the isolated molecules in the vapor phase. The observed wavenumbers for the infrared and Raman bands of

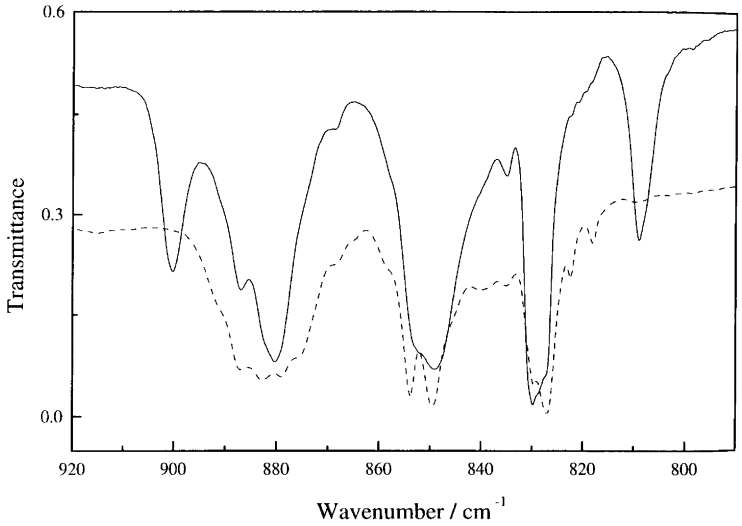

Fig. 9. Infrared spectra (920–780 cm^{-1}) of BDFS in a nitrogen matrix, unannealed (solid line) and annealed to 30 K (dashed line).

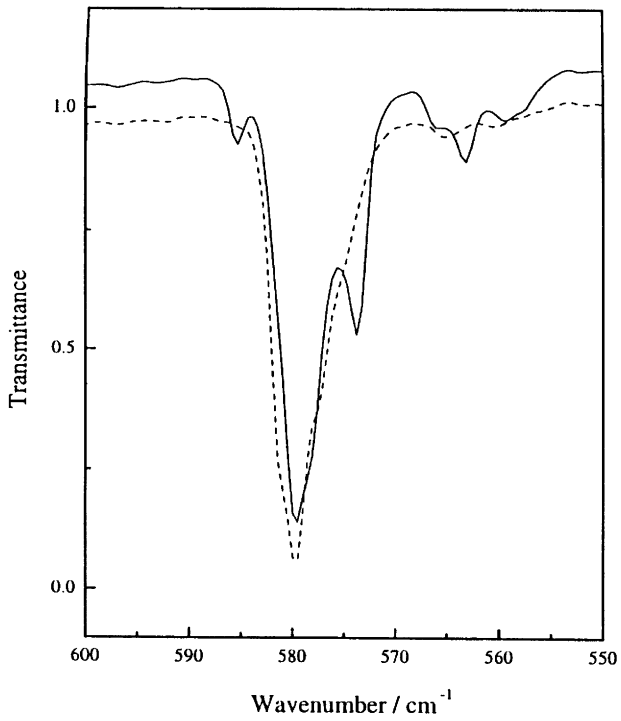

Fig. 10. Infrared spectra (590–565 cm^{-1}) of BDFS in an argon matrix, unannealed (solid line) and annealed to 36 K (dashed line).

BDFS in the various states of aggregation are listed in Table 1. The bands vanishing in the crystalline solids are denoted by asterisks. Infrared bands of BDFS in argon and nitrogen matrices are denoted by arrows pointing upwards or downwards if the bands increase or decrease in intensity after annealing, respectively.

Quantum chemical calculations. Hartree–Fock quantum chemical calculations were performed using the Gaussian-94 program.[16] A variety of approximations were employed: HF/3-21G*, HF/6-31G*, HF/6-311G*, MP2/6-31G* and MP2/6-311G*. The minima on the potential surface were found by relaxing the geometric parameters with standard optimization methods. The following conformational energies were derived: 3.7, 4.8, 4.8, 4.6 and 5.4 kJ mol^{-1}, for the basis sets listed above, respectively. All these calculations favor *anti* as the low-energy conformer, and the value 4.8 kJ mol^{-1} derived from the basis set HF/6-311G* has been employed in comparisons of BDFS with the other halomethyl dimethyl halosilanes.[17] Analytical H-F force constants were derived for each of the two conformers in BDFS, using the HF/6-311G* basis set. In addition, infrared intensities, Raman scattering cross-sections and Raman polarization ratios, ρ, were calculated.

Negligible variations in the bond distances and bond angles for the *anti* and *gauche* conformers were calculated. The Si–C bond was 189 pm for both the *anti* and *gauche* conformers in BDFS, and the same values were calculated for chloromethyl dimethyl chlorosilane.[18] The Si–F distance was 209 pm for the *anti* and 208 pm for the *gauche* conformers, at slight variance to the distances reported from *ab initio* calculations for various disilanes[9,10,19,20] employing different basis sets. The longer Si–F distance for the *anti* compared with the *gauche* conformers is in agreement with the *gauche* effect. The dipole moment of the *anti* conformer was calculated as ca. 0.8 D, while the *gauche* conformer, with a dihedral F–Si–C–Br angle of 66°, was predicted to have a much larger moment of ca. 3.4 D.

Normal coordinate calculations. The calculated *ab initio* force constants were transformed from Cartesian to symmetry coordinates, derived from a set of valence coordinates. The *ab initio* calculated wavenumbers, listed as ν_{calc} in Tables 3 and 4, are invariably higher than the experimental values. In order to make a complete assignment of the observed IR and Raman bands, a normal

Table 3. Calculated and observed fundamentals for the *anti* conformer of bromomethyl dimethyl fluorosilane (BDFS).

Vib. no.		ν_{calc}[a]	ν_{calc}[b] (scaled)	I_{IR}[c] (int.)	I_R[d] (int.)	Dep.	ν_{obs}	I_{IR}	I_R	PED[e]
ν_1	A''	3314	2983	2.9	74.4	0.75	3004	vw	m,P	$100S_{22}$
ν_2	A'	3253	2928	22.0	110.9	0.11	2971	m	m,P	$97S_5$
ν_3	A'	3249	2924	18.2	88.7	0.75	2965	w	w	$67S_8$, $30S_7$
ν_4	A''	3247	2922	4.5	27.1	0.75	2943	w	m,P	$59S_{25}$, $40S_{24}$
ν_5	A'	3238	2915	29.4	141.3	0.75	2943	w	m,P	$68S_7$, $31S_8$
ν_6	A''	3237	2913	7.4	39.6	0.75	2910	w	s,P	$59S_{24}$, $40S_{25}$
ν_7	A'	3175	2857	3.2	232.3	0.01	2910	w	s,P	$99S_6$
ν_8	A''	3173	2856	7.6	3.9	0.75	2910	w	s,P	$99S_{23}$
ν_9	A'	1600	1440	9.0	1.1	0.57	1465	w	w	$84S_{19}$
ν_{10}	A'	1596	1436	8.3	11.0	0.75	1425	w	w	$93S_{33}$
ν_{11}	A''	1588	1430	1.3	1.6	0.75	1405	m	m,P	$86S_{18}$
ν_{12}	A''	1586	1428	0.0	15.2	0.75	1405	m	m,P	$93S_{34}$
ν_{13}	A'	1573	1416	18.8	13.2	0.72	1390	w	m	$90S_{13}$
ν_{14}	A'	1452	1307	29.5	2.4	0.05	1277	s	vw	$95S_{15}$
ν_{15}	A''	1447	1302	57.6	0.2	0.75	1260	vs	m,P	$94S_{30}$
ν_{16}	A'	1293	1164	10.9	2.7	0.74	1132	m	m	$90S_{14}$
ν_{17}	A''	1180	1062	3.8	5.1	0.75	1049	m	w	$96S_{28}$
ν_{18}	A'	965	869	140.8	0.6	0.68	877	vs	w	$38S_{16}$, $32S_3$, $11S_{17}$
ν_{19}	A'	945	850	185.9	0.4	0.22	849[f]	s		$43S_{17}$, $24S_{16}$
ν_{20}	A''	909	818	139.4	0.1	0.75	828	s	w	$28S_{31}$, $30S_{29}$, $25S_{21}$
ν_{21}	A'	850	765	36.9	1.5	0.74	775	s	w,P	$54S_3$, $19S_{17}$, $15S_{16}$
ν_{22}	A''	842	758	14.4	1.5	0.75	753	m	vw	$77S_{32}$
ν_{23}	A'	788	709	19.8	7.2	0.55	736	m	w	$65S_2$
ν_{24}	A''	756	680	7.6	3.4	0.75	700	m	m	$53S_{21}$, $42S_{31}$
ν_{25}	A''	727	654	0.1	1.7	0.75	665	w	w	$52S_{29}$, $14S_{31}$, $12S_{32}$, $11S_{28}$
ν_{26}	A'	669	602	25.3	11.7	0.65	641	m	s,P	$50S_1$, $33S_4$
ν_{27}	A'	598	538	20.7	28.2	0.05	576	m	vs,P	$39S_4$, $26S_1$, $18S_{12}$
ν_{28}	A''	293	293	19.0	1.1	0.75	284	s	m,D	$62S_{26}$, $13S_{27}$, $10S_{31}$
ν_{29}	A'	290	290	20.1	0.3	0.65	274[f]	s	m	$19S_{10}$, $24S_9$, $16S_{12}$, $12S_{11}$
ν_{30}	A'	255	255	8.8	1.8	0.58	237		m,P	$36S_9$, $17S_{11}$, $13S_{10}$, $13S_{16}$
ν_{31}	A''	206	206	7.5	0.3	0.75	210	w	w	$58S_{27}$, $20S_{26}$
ν_{32}	A'	202	202	0.3	1.6	0.51	198		m,P	$41S_{11}$, $28S_{10}$, $11S_{16}$
ν_{33}	A'	150	150	0.0	0.1	0.20	176[f]	w	w	$85S_{20}$
ν_{34}	A''	143	143	0.2	0.0	0.75	148[g]	w	w	$93S_{36}$
ν_{35}	A'	113	113	3.6	0.6	0.72	115	vw	w,P	$54S_{12}$, $23S_{13}$
ν_{36}	A''	62	62	3.0	1.6	0.75	77	w	m	$84S_{35}$, $13S_{36}$

[a]Calculated with basis set HF/6-311G*. [b]Scaled with a factor of 0.9 above and 1.0 below 400 cm^{-1}. [c]Calculated infrared intensities (km mol^{-1}). [d]Calculated Raman cross-sections ($Å^4$ mol^{-1}). [e]Terms below 10% are omitted. [f]IR spectrum of the amorphous solid. [g]Raman spectrum of the crystal.

coordinate analysis with scaled force constants was carried out.

Various scaling factors applied to the different types of motions were tested. However, equally good agreement between the experimental and calculated wavenumbers was achieved by using scaling factors of 0.9 for the stretching and bending modes above, and 1.0 for the modes below 400 cm^{-1}. In addition, infrared intensities, Raman scattering cross-sections and Raman polarization ratios, ρ, were calculated, and these data are contained in Tables 3 and 4.

The PED (potential energy distribution) listed in Tables 3 and 4 are expressed in terms of the symmetry coordinates (Table 5) and are defined from the internal coordinates for BDFS given in Fig. 11. Only PED terms larger than 10% have been included in Tables 3 and 4. The C–H, C–Br and Si–F stretching modes are reasonably well localized, but the CH_3 rock, C–C stretches and the skeletal deformations are highly mixed.

Discussion

Conformations. As is apparent from Table 1, the bands around 1132, 1049, 877, 736, 576, 284 and 198 cm^{-1} vanish during crystallization both in the infrared and Raman spectra. In addition, the Raman band at 237 cm^{-1} with no infrared counterpart disappears and so does the band at 828 cm^{-1}. However, the latter has an infrared analogue that still remains in the crystal at 826 cm^{-1}. These bands undoubtedly belong to the conformer which disappears in the crystal, supported by the fact that they are enhanced in the argon and nitrogen matrix spectra after annealing. Finally these bands are also enhanced in intensity with temperature as observed in the Raman spectra of the liquid.

The essential question remains: do these bands belong to the *anti* or *gauche* conformer? The fact that the *ab initio* quantum chemical calculations gave enthalpy differences between 3.7 and 5.4 kJ mol^{-1} depending on

Table 4. Calculated and observed fundamentals for the *gauche* conformer of bromomethyl dimethyl fluorosilane (BDFS).

Vib. no.	ν_{calc}[a]	ν_{calc}[b] (scaled)	I_{IR}[c] (int.)	I_R[d] (int.)	Dep.	ν_{obs}	I_{IR}	I_R	PED[e]
ν_1	3301	2971	3.8	67.3	0.72	3004	m	m,P	$99S_{22}$
ν_2	3257	2931	11.8	68.1	0.74	2971	m	m,P	$49S_7$, $47S_{24}$
ν_3	3243	2919	19.4	102.5	0.18	2965	w	m,P	$96S_5$
ν_4	3238	2914	19.2	97.5	0.71	2943	w	m,P	$44S_{24}$, $41S_7$
ν_5	3233	2910	35.9	134.3	0.65	2943	w	m,P	$86S_8$
ν_6	3230	2907	2.0	21.6	0.70	2910	w	s,P	$92S_{25}$
ν_7	3173	2856	6.8	158.4	0.01	2910	w	s,P	$69S_6$, $28S_{23}$
ν_8	3168	2851	6.6	75.1	0.00	2910	w	s,P	$70S_{23}$, $29S_6$
ν_9	1601	1441	14.9	2.5	0.74	1465	w	w	$86S_{19}$
ν_{10}	1593	1434	3.2	14.5	0.75	1425	m	vw	$83S_{18}$
ν_{11}	1589	1430	1.7	9.2	0.75	1405	m	m,P	$55S_{34}$, $38S_{33}$
ν_{12}	1585	1427	1.5	9.1	0.75	1405	m	m,P	$51S_{33}$, $41S_{34}$
ν_{13}	1570	1413	16.5	8.8	0.67	1390	w	m	$91S_{13}$
ν_{14}	1451	1306	32.0	2.7	0.05	1277	s	vw	$93S_{15}$
ν_{15}	1446	1301	51.8	0.3	0.23	1260	vs	m,P	$92S_{30}$
ν_{16}	1302	1172	14.3	3.4	0.68	1141	m	w,P	$90S_{14}$
ν_{17}	1194	1175	2.2	5.6	0.75	1057	m	w,P	$96S_{28}$
ν_{18}	979	881	179.1	0.4	0.46	877	vs	w,P	$43S_3$, $21S_{17}$, $14S_{16}$
ν_{19}	948	853	165.1	1.0	0.50	849[f]	vs		$50S_{16}$, $23S_{17}$, $12S_2$
ν_{20}	879	792	113.6	0.8	0.56	810	s	w,P	$38S_{31}$, $33S_{21}$
ν_{21}	855	770	26.0	1.5	0.73	775	s	w,P	$53S_3$, $25S_{17}$, $14S_{16}$
ν_{22}	833	750	10.3	1.5	0.71	753	m	vw	$83S_{32}$
ν_{23}	784	706	11.0	13.7	0.36	723	m	m,P	$42S_2$, $17S_4$, $11S_{31}$
ν_{24}	750	675	12.1	5.9	0.70	700	m	m	$56S_{21}$, $31S_{31}$
ν_{25}	738	664	3.7	4.5	0.64	665	w	w	$51S_{29}$, $10S_2$
ν_{26}	668	601	16.2	5.9	0.27	641	m	s,P	$57S_1$, $20S_4$, $12S_2$
ν_{27}	588	529	11.2	28.2	0.12	560	m	vs,P	$35S_4$, $21S_{12}$, $16S_1$
ν_{28}	331	298	40.1	2.8	0.44	315	s	m,P	$27S_{10}$, $13S_{12}$, $13S_{26}$, $10S_{11}$
ν_{29}	288	288	21.4	1.1	0.67	274[f]	s	m,D	$44S_{26}$, $20S_{10}$
ν_{30}	239	239	0.8	1.3	0.40	248	m	m,P	$69S_9$, $12S_{17}$
ν_{31}	204	204	0.4	0.2	0.72	210	w	w	$38S_{11}$, $22S_{10}$, $11S_{27}$
ν_{32}	192	192	0.1	2.3	0.51	191	m	m,P	$29S_{27}$, $19S_{26}$, $17S_{11}$
ν_{33}	158	158	0.1	0.1	0.38	173[f]	w	w	$76S_{20}$
ν_{34}	146	146	0.1	0.1	0.66	148[f]	w	w	$87S_{36}$
ν_{35}	111	111	0.4	0.3	0.71	115	vw	w,P	$50S_{12}$, $23S_{13}$, $16S_{27}$
ν_{36}	57	57	1.6	0.7	0.74	77	w	m	$80S_{35}$

For abbreviations, see footnotes to Table 3.

the level of approximation (see above) with *anti* as the low-energy conformer, will not be regarded as conclusive in itself. It should be noted though, that in the series of five molecules with the structure $CH_2X(CH_3)_2SiY$ investigated so far, *anti* was invariably calculated[17] to be the low-energy conformer at the HF/6-311G* level with values ranging from 7.4 to 1.3 kJ mol^{-1}.

The *anti* conformer has C_s symmetry provided that the six hydrogens in the two methyl groups are oriented symmetrically to the symmetry plane, while the *gauche* conformer has no symmetry (Fig. 1). The 36 fundamentals in the *anti* conformer will divide themselves between 20 of symmetry species A' and 16 of species A'' of which the former will give rise to polarized, the latter to depolarized bands in the Raman spectra. In the *gauche* conformer without symmetry all the 36 fundamentals will obviously give rise to polarized Raman bands. Because of the low symmetry and since the majority of *anti* and *gauche* bands overlap (ca. seven bands of each conformer appear separate) these criteria are of limited value in the assignment. Another clue is the rotational fine structures in the infrared vapor spectra, since they should be slightly different for the *anti* and *gauche* conformers. However, as is apparent from Figs. 4 and 5 the vapor contours are ill defined: a possible exception might be the infrared band at 642 cm^{-1} with an apparent A-type contour and shoulder separation of 9 cm^{-1}. However, the assignments as well as the results of the force constant calculations indicate that these peaks are not caused by rotational fine structure, but are due to partly overlapping *anti* and *gauche* fundamentals ν_{26}.

It remains to correlate the infrared and Raman bands vanishing in the crystal with the scaled *ab initio* wavenumbers for the *anti* (Table 3) and *gauche* (Table 4) fundamentals. Outside the typical group frequency regions for the CH_3 and CH_2 stretching and deformation vibrations where the calculated wavenumbers for the *anti* and *gauche* fundamentals overlap, some significant frequency differences were calculated. Thus, below 1200 cm^{-1} there are nine instances in which the calculated *anti* and *gauche* fundamentals are separated by more than 10 cm^{-1}, and it is significant that the observed

Table 5. Symmetry coordinates for bromomethyl dimethyl fluorosilane (BDFS).

A'		
1	Si–C symmetric stretch	$S_1 = 3^{-1/2}(R_1 + R_2 + R_3)$
2	Si–C antisymmetric stretch	$S_2 = 6^{-1/2}(2R_1 - R_2 - R_3)$
3	Si–F stretch	$S_3 = S$
4	C–Br stretch	$S_4 = T$
5	CH_2 symmetric stretch	$S_5 = 2^{-1/2}(s_7 + s_8)$
6	CH_3 symmetric stretch	$S_6 = 6^{-1/2}(d_1 + d_2 + d_3 + d_4 + d_5 + d_6)$
7	CH_3 antisymmetric stretch	$S_7 = 12^{-1/2}(2d_1 - d_2 - d_3 + 2d_4 - d_5 - d_6)$
8	CH_3 antisymmetric stretch	$S_8 = \frac{1}{2}(d_2 - d_3 + d_5 - d_6)$
9	Symmetric C–Si–C bend	$S_9 = 6^{-1/2}(\Xi_1 + \Xi_2 + \Xi_3 - \Phi_1 - \Phi_2 - \Phi_3)$
10	Antisymmetric C–Si–C bend	$S_{10} = 6^{-1/2}(2\Xi_1 - \Xi_2 - \Xi_3)$
11	Antisymmetric C–Si–C bend	$S_{11} = 6^{-1/2}(2\Phi_1 - \Phi_2 - \Phi_3)$
12	Si–C–Br bend	$S_{12} = \Omega$
13	CH_2 scissor	$S_{13} = \frac{1}{2}(\gamma_1 + \gamma_2 + \theta_1 + \theta_2)$
14	CH_2 wag	$S_{14} = \frac{1}{2}(\gamma_1 + \gamma_2 - \theta_1 - \theta_2)$
15	CH_3 symmetric deformation	$S_{15} = 12^{-1/2}(\beta_1 + \beta_2 + \beta_3 - \alpha_1 - \alpha_2 - \alpha_3 + \beta_4 + \beta_5 + \beta_6 - \alpha_4 - \alpha_5 - \alpha_6)$
16	CH_3 antisymmetric deformation	$S_{16} = 12^{-1/2}(2\beta_1 - \beta_2 - \beta_3 + 2\beta_4 - \beta_5 - \beta_6)$
17	CH_3 antisymmetric deformation	$S_{17} = \frac{1}{2}(\beta_2 - \beta_3 + \beta_5 - \beta_6)$
18	CH_3 antisymmetric deformation	$S_{18} = 12^{-1/2}(2\alpha_1 - \alpha_2 - \alpha_3 + 2\alpha_4 - \alpha_5 - \alpha_6)$
19	CH_3 antisymmetric deformation	$S_{19} = \frac{1}{2}(\alpha_2 - \alpha_3 + \alpha_5 - \alpha_6)$
20	CH_3 torsion	$S_{20} = 2^{-1/2}(\tau_2 + \tau_3)$
A''		
21	Si–C antisymmetric stretch	$S_{21} = 2^{-1/2}(R_2 - R_3)$
22	CH_2 antisymmetric stretch	$S_{22} = 2^{-1/2}(s_7 - s_8)$
23	CH_3 symmetric stretch	$S_{23} = 6^{-1/2}(d_1 + d_2 + d_3 - d_4 - d_5 - d_6)$
24	CH_3 antisymmetric stretch	$S_{24} = 12^{-1/2}(2d_1 - d_2 - d_3 - 2d_4 + d_5 + d_6)$
25	CH_3 antisymmetric stretch	$S_{25} = \frac{1}{2}(d_2 - d_3 - d_5 + d_6)$
26	C–Si–F deformation	$S_{26} = 2^{-1/2}(\Xi_2 - \Xi_3)$
27	C–Si–C deformation	$S_{27} = 6^{-1/2}(\Phi_2 - \Phi_3)$
28	CH_2 twist	$S_{28} = \frac{1}{2}(\gamma_1 - \gamma_2 - \theta_1 + \theta_2)$
29	CH_2 rock	$S_{29} = \frac{1}{2}(\gamma_1 - \gamma_2 + \theta_1 - \theta_2)$
30	CH_3 symmetric deformation	$S_{30} = 12^{-1/2}(\beta_1 + \beta_2 + \beta_3 - \alpha_1 - \alpha_2 - \alpha_3 - \beta_4 - \beta_5 - \beta_6 + \alpha_4 + \alpha_5 + \alpha_6)$
31	CH_3 antisymmetric deformation	$S_{31} = 12^{-1/2}(2\beta_1 - \beta_2 - \beta_3 - 2\beta_4 + \beta_5 + \beta_6)$
32	CH_3 antisymmetric deformation	$S_{32} = \frac{1}{2}(\beta_2 - \beta_3 - \beta_5 + \beta_6)$
33	CH_3 antisymmetric deformation	$S_{33} = 12^{-1/2}(2\alpha_1 - \alpha_2 - \alpha_3 - 2\alpha_4 + \alpha_5 + \alpha_6)$
34	CH_3 antisymmetric deformation	$S_{34} = \frac{1}{2}(\alpha_2 - \alpha_3 - \alpha_5 + \alpha_6)$
35	CH_2Br torsion	$S_{35} = \tau_1$
36	CH_3 torsion	$S_{36} = 2^{-1/2}(\tau_2 - \tau_3)$

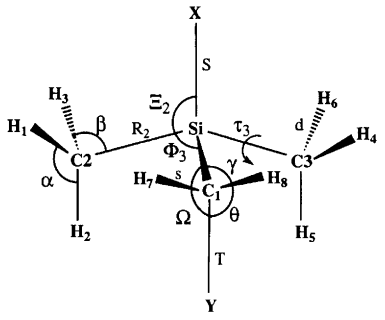

Fig. 11. Valence coordinates for BDFS.

anti/gauche band pairs generally appear at these frequencies.

The following nine observed band pairs: 1132*/1141, 1049*/1057, 877*/853, 828*/810, 736*/723, 576*/561, 284*/315, 237*/248 and 198*/191 cm^{-1} (the bands with asterisks vanished in the IR and/or Raman spectra) were correlated with the scaled, calculated wavenumbers of the *anti* and *gauche* conformers (Tables 3 and 4). It was found that in seven instances the bands with asterisks were fitted with *anti* and the remaining bands with *gauche*, while for two band pairs the opposite correlation was preferred. Also, the experimental and calculated shifts were in reasonable agreement for these seven band pairs. In the two exceptions, 877*/853 and 237*/248 cm^{-1}, the bands with asterisks were preferably correlated with *gauche*, the remaining band with *anti*. However, it should be emphasized that these band pairs are not as certain as the others. Thus, the 872 cm^{-1} band appeared on a falling background in the IR spectra and the 878 cm^{-1} Raman band was quite weak, making the disappearance somewhat uncertain. The 235 cm^{-1} Raman band definitely vanished in the crystal, but no IR counterpart was observed (Table 1).

In spite of the two inconsistencies noted, we feel that there are good reasons to assign the vanishing bands with *anti*, meaning that the *gauche* conformer remains in the crystal and is the low-energy conformer in the liquid. Some additional arguments support this conclusion: (1) In chloromethyl dimethyl fluorosilane,[15] in which the vibrational spectra and conformations are very similar to those of BDFS, the experimentally determined band pairs revealed with one possible exception that *gauche* was present in the crystal, similar to the conclusion for

BDFS. (2) Considering the low enthalpy difference between the conformers in the liquid (0.4 kJ mol^{-1} with *gauche* having the lower energy) it is expected that the *anti* conformer may be the more stable conformer in the vapor, and probably in the matrices as well, in agreement with the experimental results. The bond moments of C–Br and Si–F are much larger than for the other bonds in BDFS. Therefore the *anti* conformer with opposite C–Br and Si–F bonds has a much lower dipole moment (calculated as 0.8 D) than *gauche* (calculated as 3.4 D), in which these bonds make approximately a tetrahedral angle. A stabilization of the polar conformer in polar solvents and in the liquid compared to the vapor, has been observed for numerous conformational systems,[21] and agrees with the dielectric theory first proposed by Onsager.[22] Therefore, while *anti* is the low energy conformer in the matrices and presumably in the vapor, the stabilization of the polar *gauche* molecule in the liquid leads to *gauche* being the low-energy conformer in the latter. Again, the findings in chloromethyl dimethyl fluorosilane[15] are in complete agreement with the present results.

Spectral assignments. The assignments of the infrared and Raman spectra of BDFS to the *anti* and *gauche* conformers appear in Tables 1, 3 and 4 and need to be discussed only in special cases. In order to maintain the similarity between the two conformers, the fundamentals of both *anti* and *gauche* have been numbered consecutively rather than the conventional numbering of the modes belonging to species *A′* before those of *A″* in the *anti* conformer. With six hydrogens belonging to methyl and two to methylene groups we expect eight C–H stretching fundamentals ν_1–ν_8 of each conformer. Some of these are accidentally degenerate, and moreover the fundamentals of *anti* overlap those of *gauche*. These modes were assigned to infrared and Raman bands between 3008 and 2915 cm^{-1}. A number of vibrational modes involving asymmetric and symmetric CH_3 deformation and the CH_2 scissor and wagging modes are expected below 1470 cm^{-1}. The *ab initio* calculations reveal that the *anti* and *gauche* bands should be situated between 1440 and 1280 cm^{-1} and strongly overlap in this region. We have assigned ν_9–ν_{15} for the two conformers to the bands present both in the infrared and Raman spectra at 1465, 1425, 1405, 1390, 1277 and 1260 cm^{-1} (wavenumbers of the Raman bands in the liquid are given), respectively. Most of these bands were medium or weak in intensity, an exception being the bands at 1260 cm^{-1} assigned to ν_{15}, which are very intense in the infrared spectra. In some of these cases the *anti* and *gauche* bands might be separated in the infrared matrix spectra; as an example ν_{14} is supposedly separated into 1276 *anti* and 1270 cm^{-1} *gauche* in the argon matrix.

Both the modes ν_{16} and ν_{17} form *anti* and *gauche* band pairs as clearly seen from the spectra and in good agreement with the calculations. Since no fundamentals are expected between 1040 and 900 cm^{-1} the bands in this region, some of them intense in the infrared and some disappearing in the Raman crystal spectra, must be due to combination bands or overtones. The band pair at 877 and 853 cm^{-1} was tentatively attributed to *anti* and *gauche* fundamentals of ν_{18}, respectively, but as discussed above this result is contradicted by the calculations and the assignment might be changed.

The ν_{19} mode is attributed to bands around 840 cm^{-1} in the matrices and may overlap ν_{18} (*gauche*) in the condensed state. Also, the band pair at 828 and 810 cm^{-1} is assigned to ν_{20} of the *anti* and *gauche* conformers although the former band is still present in the infrared crystal spectrum. However, this band vanishes in the Raman spectrum of the crystal; the present interpretation agrees with the intensity variations with temperature in the liquid and with changes in the matrix spectra after annealing. While ν_{23} is attributed to the band pair at 736 and 723 cm^{-1} the remaining modes between ν_{21} and ν_{26} all appear as coinciding *anti* and *gauche* bands.

The two intense Raman bands at 576 and 561 cm^{-1} and their infrared counterparts form a band pair for the mode ν_{27} (C–Br stretch). In chloromethyl dimethyl fluorosilane[15] the corresponding C–Cl stretches are situated at 607 and 598 cm^{-1}. Tentatively, ν_{28} for *anti* and *gauche* are assigned to the bands at 315 and 284 cm^{-1}, in good agreement with the large shift calculated for these bands. However, partly due to overlap of ν_{29} assigned at 278 cm^{-1} in the crystal, the disappearance of ν_{28} (*anti*) in the infrared and Raman crystal spectra seems uncertain. The Raman band at 237 cm^{-1} without an infrared counterpart definitely vanishes in the crystal spectra and is assigned as ν_{30} (*anti*), making a pair with 246 cm^{-1} ν_{30} (*gauche*) but contradicted by the calculations (see above). The pair of Raman bands at 198 and 191 cm^{-1} with uncertain, very weak infrared counterparts form *anti* and *gauche* bands of ν_{32}. Very uncertain Raman bands at 173 and 148 cm^{-1} observed in the crystal are attributed to ν_{33} and ν_{34}, while distinct infrared and Raman bands around 120 cm^{-1} are assigned as ν_{35}. Finally, weak infrared bands around 100 cm^{-1} are assigned as coinciding torsional bands of *gauche* and *anti* ν_{36}. In the $R(\nu)$ representation[23] of the liquid an uncertain Raman band was observed around 81 cm^{-1}, possibly due to ν_{36} (*anti*). An uncertain vapour band at 66 cm^{-1} observed in the infrared spectrum might be described to the second (*gauche*) conformer of ν_{36}.

Acknowledgments. We are grateful to Mrs. Anne Horn for valuable assistance. V.A. acknowledges a grant from the Norwegian Research Council reserved for the Baltic Countries and North West Russia.

References

1. Qtaitat, M. A. and Durig, J. R. *Spectrochim. Acta, Part A 49* (1993) 2139.
2. Afifi, M. S, Guirgis, G. A., Mohamed, T. A., Herrebout, W. A. and Durig, J. R. *J. Raman Spectrosc. 25* (1994) 159.

3. Durig, J. R., Guirgis, G. A., Mohamed, T. A., Herrebout, W. A. and Afifi, M. S. *J. Mol. Struct. 319* (1994) 109.
4. Durig, R. J., Sullivan, J. F., Guirgis, G. A. and Qtaitat, M. A. *J. Phys. Chem. 95* (1991) 1563.
5. Durig, R. J., Guirgis, G. A. and Qtaitat, M. A. *J. Raman Spectrosc. 26* (1995) 413.
6. Durig, R. J., Guirgis, G. A., Kim, Y. H., Yan, W. and Qtaitat, M. A. *J. Mol. Struct. 382* (1996) 111.
7. Hassler, K., Köll, W. and Schenzel, K. *J. Mol. Struct. 348* (1995) 353.
8. Ernst, M., Schenzel, K., Jähn, A. and Hassler, K. *J. Mol. Struct. 412* (1997) 83.
9. Ernst, M., Schenkel, K., Jähn, A., Köll, W. and Hassler, K. *J. Raman Spectrosc. 28* (1997) 589.
10. Schenzel, K. and Hassler, K. *Spectrochim. Acta, Part A 52* (1996) 637.
11. Jensen, H. M., Klaeboe, P., Nielsen, C. J., Aleksa, V., Guirgis, G. A. and Durig, J. R. *J. Mol. Struct. 410–411* (1997) 489.
12. Speier, J. *J. Am. Chem. Soc. 73* (1951) 826.
13. Miller, F. A. and Harney, B. M. *Appl. Spectrosc. 24* (1970) 291.
14. Barnes, A. J. *J. Mol. Struct. 113* (1984) 161.
15. Aleksa, V., Klaeboe, P., Nielsen, C. J. and Guirgis, G. A. *J. Mol. Struct. 445* (1998) 161.
16. Frisch, M. J., Trucks, G. W., Schlegel, H. B., Gill, P. M. W., Johnson, B. G., Robb, M. A., Cheeseman, J. R., Keith, T., Petersson, G. A., Montgomery, J. A., Raghavachari, K., Al-Laham, M. A., Zakrzewski, V. G., Ortiz, J. V., Foresman, J. B., Cioslowski, J., Stefanov, B. B., Nanayakkara, A., Challacombe, M., Peng, C. Y., Ayala, P. Y., Chen, W., Wong, M. W., Andre, J. L., Replogle, E. S., Martin, R. L., Fox, D. J., Binkley, J. S., Defrees, D. J., Baker, J., Stewart, J. P., Head-Gordon, M., Gonzalez, C. and Pople, J. A., *Gaussian 94, Revision D.2*, Gaussian, Inc., Pittsburgh, PA 1995.
17. Klaeboe, P. *J. Mol. Struct. 408–409* (1997) 81.
18. Jensen, H. M., Klaeboe, P., Guirgis, G. A., Aleksa, V., Nielsen, C. J. and Durig, J. R. *J. Mol. Struct. 410–411* (1997) 483.
19. McKean, D. C., McPhail, A. L., Edwards, H. G. M., Lewis, I. R., Mastryukov, V. and Boggs, J. E. *Spectrochim. Acta, Part A 49* (1993) 1079.
20. McKean, D. C., Edwards, H. G. M., Lewis, I. R., Murphy, W. F., Mastryukov, V. and Boggs, J. E. *Spectrochim. Acta, Part A 51* (1995) 2237.
21. Abraham, R. J. and Bretschneider, E. In: Orville-Thomas, W. J., Ed. *Internal Rotation in Molecules.* Wiley, London 1974.
22. Onsager, L. *J. Am. Chem. Soc. 58* (1936) 1486.
23. Faurskov Nielsen, O. *Annu. Rep. Progr. Chem., Sect. C, Phys. Chem. 90* (1993) 3.

Received January 16, 1998.